GA–A27429

INTEGRATED MAGNETIC AND KINETIC CONTROL OF ADVANCED TOKAMAK SCENARIOS BASED ON DATA-DRIVEN MODELS

by
D. MOREAU, M.L. WALKER, J.R. FERRON, F. LIU, E. SCHUSTER, J.F. ARTAUD, J.E. BARTON, D. BOYER, K.H. BURRELL, S.M. FLANAGAN, J. GARCIA, P. GOHIL, R.J. GROEBNER, C.T. HOLCOMB, D.A. HUMPHREYS, A.W. HYATT, R.D. JOHNSON, R.J. LA HAYE, J. LOHR, T.C. LUCE, R. NOUAILLETAS, J.M. PARK, B.G. PENAFLOR, W. SHI, F. TURCO, W. WEHNER, and ITPA-IOS Group Members and Experts

OCTOBER 2012

GENERAL ATOMICS

DISCLAIMER

GA–A27429

INTEGRATED MAGNETIC AND KINETIC CONTROL OF ADVANCED TOKAMAK SCENARIOS BASED ON DATA-DRIVEN MODELS

by
D. MOREAU,* M.L. WALKER, J.R. FERRON, F. LIU,* E. SCHUSTER,† J.F. ARTAUD,* J.E. BARTON,† D. BOYER,† K.H. BURRELL, S.M. FLANAGAN, J. GARCIA,* P. GOHIL, R.J. GROEBNER, C.T. HOLCOMB,‡ D.A. HUMPHREYS, A.W. HYATT, R.D. JOHNSON, R.J. LA HAYE, J. LOHR, T.C. LUCE, R. NOUAILLETAS,* J.M. PARK,# B.G. PENAFLOR, W. SHI,† F. TURCO,§ W. WEHNER,† and ITPA-IOS Group Members and Experts

This is a preprint of a paper to be presented at the Twenty-fourth IAEA Fusion Energy Conf., October 8-13, 2012 in San Diego, California.

*CEA, IFRM, 13108 Saint-Paul-lez-Durance, France.
†Lehigh University, Bethlehem, Pennsylvania.
‡Lawrence Livermore National Laboratory, Livermore, California.
#Oak Ridge National Laboratory, Oak Ridge, Tennessee.
§Columbia University, New York, New York.

Work supported in part by
the U.S. Department of Energy
under DE-FC02-04ER54698, DE-FG02-09ER55064, DE-AC52-07NA27344,
DE-AC05-00OR22725, DE-FG02-04ER54761, and by
the European Fusion Development Agreement

GENERAL ATOMICS PROJECT 30200
OCTOBER 2012

GENERAL ATOMICS

Integrated Magnetic and Kinetic Control of Advanced Tokamak Scenarios Based on Data-Driven Models

D. Moreau 1), M.L. Walker 2), J.R. Ferron 2), F. Liu 1), E. Schuster 3), J.F. Artaud 1), J.E. Barton 3), M.D. Boyer 3), K.H. Burrell 2), S.M. Flanagan 2), J. Garcia 1), P. Gohil 2), R.J. Groebner 2), C.T. Holcomb 4), D.A. Humphreys 2), A.W. Hyatt 2), R.D. Johnson 2), R.J. La Haye 2), J. Lohr 2), T.C. Luce 2), R. Nouailletas 1), J.M. Park 5), B.G. Penaflor 2), W. Shi 3), F. Turco 6), W. Wehner 3), and ITPA-IOS group members and experts

1) CEA, IRFM, 13108 Saint-Paul-lez-Durance, France
2) General Atomics, PO Box 85608, San Diego, CA 92186-5608, USA
3) Lehigh University, Bethlehem, PA 18015, USA
4) Lawrence Livermore National Laboratory, 7000 East Ave, Livermore, CA 94550, USA
5) Oak Ridge National Laboratory, PO Box 2008, Oak Ridge, TN 37831, USA
6) Columbia University, 116th St and Broadway, New York, NY 10027, USA

E-mail contact of main author: didier.moreau@cea.fr

Abstract. The first real-time profile control experiments integrating magnetic and kinetic variables were performed on DIII-D in view of regulating and extrapolating advanced tokamak scenarios to steady state devices and burning plasma experiments. Device-specific, control-oriented models were obtained from experimental data and these data-driven models were used to synthesize integrated magnetic and kinetic profile controllers. Closed-loop experiments were performed for the regulation of (a) the poloidal flux profile, $\Psi(x)$, (b) the inverse of the safety factor profile, $\iota(x)=1/q(x)$, and (c) either the $\Psi(x)$ profile or the $\iota(x)$ profile together with the normalized pressure parameter, β_N. The neutral beam injection (NBI), electron cyclotron current drive (ECCD) systems and ohmic coils provided the heating and current drive (H&CD) sources. The first control actuator was the plasma surface loop voltage or current (i. e. the ohmic coil), and the available beamlines and gyrotrons were grouped to form five additional H&CD actuators: co-current on-axis NBI, co-current off-axis NBI, counter-current NBI, balanced NBI and total ECCD power from all gyrotrons (with off-axis current deposition). The control method was also applied on simulated ITER discharges using a simplified transport code (METIS).

1. Introduction

The development on ITER of hybrid and steady state operation scenarios with high neutron fluence implies the control of improved-confinement, high-β, high-bootstrap discharges. Such discharges are obtained in the so-called advanced tokamak (AT) operation scenarios in which an optimization of some plasma parameter profiles results in a large improvement in fusion performance, at reduced plasma current. A high-gain fusion burn could then be achieved with extended pulse length in a burning plasma device such as ITER, a major fraction of the toroidal current being self-generated by the neoclassical bootstrap effect. The ongoing research on AT scenarios is important for the development of a steady state tokamak reactor

Without adequate profile control, AT plasmas are currently obtained in various devices empirically [1-3], and most of the time transiently or for durations that do not exceed the resistive diffusion time. The high plasma performance phase is often limited in duration by transport and MHD phenomena. Extensive work has been dedicated in recent years to the control of MHD instabilities, such as the neo-classical tearing modes (NTM) or resistive wall modes (RWM), but integrated magnetic and kinetic control of plasma profiles and parameters such as the current profile, the pressure profile (or the normalized pressure parameter, β_N) and, in ITER, the alpha-particle power, are also essential for the extrapolation of the scenarios to long-pulse or steady state operation. In present-day devices, the regulation of plasma

parameter profiles is also motivated by the potential gain that it could yield in running stable and reproducible discharges, in order to study the physics of AT scenarios for ITER.

An integrated model-based plasma control approach has been initiated on JET [4] and pursued on JT-60U and DIII-D [5-7], under the framework of the International Tokamak Physics Activity for Integrated Operation Scenarios (ITPA-IOS). It relies on generic, data-driven, system identification techniques and on singular perturbation control methods [8]. The algorithm to determine the device-specific, control-oriented (approximate) models that are needed for controller design was developed and validated using data from these three tokamaks [4-5] (see Sec. 4 for specifics of the DIII-D model), and also using data obtained from ITER simulations [9]. Data-driven control-oriented models were subsequently used to synthesize integrated controllers for the simultaneous control of the current profile and of β_N in the DIII-D high-β_N steady state scenario, and for current profile and burn control simulations in the ITER hybrid scenario. The DIII-D Plasma Control System (PCS) has been upgraded for these experiments and its control capability has been expanded to include the possibility of simultaneously controlling the evolution of one magnetic radial profile such as the internal poloidal flux, $\Psi(x)$, the safety factor, $q(x)$, its inverse, $\iota(x)$, or $d\Psi/dx$, and up to two kinetic profiles (e.g. toroidal rotation and ion temperature) and one scalar parameter such as the normalized pressure parameter, β_N. Two controllers based on data-driven models with slightly different algorithms, were tested. Sections 2 and 3 describe the choice of the relevant state variables, the structure of the reduced state-space models and the main features of the two control algorithms. Then in the following sections, the experimental results for the control of $\Psi(x)$, $\iota(x)$, and the simultaneous control of $\Psi(x)$ or $\iota(x)$, and β_N will be described. The last section deals with the application of the control scheme to ITER using simulations.

2. Two-time-scale State-space Structure of the Dynamic Plasma Models

In a tokamak, the multiple parameter profiles that define the plasma state (poloidal magnetic flux, safety factor, plasma density, velocity, pressure, etc.) are known to be strongly and nonlinearly coupled. However, because of this coupling, the profiles that need be controlled in real-time to reach a given equilibrium and regulate the plasma around that state may be reduced to a minimal set of essential ones. In the control approach followed here, the coupling between magnetic and kinetic plasma parameters and profiles is given more emphasis in the controller synthesis than the non-linearity of the system. Nonlinear plasma models are too complex and still too uncertain to be readily integrated in a profile controller design. However, well-identified nonlinearities could be taken into account in the future, if needed.

Thus, based on the structure of flux-averaged transport equations, a control-oriented, grey box, state space plasma model is postulated to consist of a set of strongly coupled linearized plasma response equations that only depends on the normalized radius x and time t [4-5]:

$$\frac{\partial \Psi(x,t)}{\partial t} = \mathcal{L}_{\Psi,\Psi}\{x\} \bullet \Psi(x,t) + \mathcal{L}_{\Psi,K}\{x\} \bullet X + L_{\Psi,P}(x) \cdot P(t) + V_{ext}(t) \quad (1)$$

$$\varepsilon \frac{\partial}{\partial t} X = \mathcal{L}_{K,\Psi}\{x\} \bullet \Psi(x,t) + \mathcal{L}_{K,K}\{x\} \bullet X + \mathcal{L}_{K,P}(x) \cdot P(t) \quad (2)$$

Here, the magnetic flux, $\Psi(x,t)$, and a set of kinetic profiles and scalar parameters represented by the vector X (such as density, toroidal velocity, ion and electron temperatures, or β_N and, in a burning plasma, the alpha-particle power, P_α) appear as the most natural state variables of the system for our purposes. The system is linearized around an equilibrium state which is

called the reference state, and *which needs not be known explicitly*. The radial variable, x, is defined as $(\Phi/\Phi_{max})^{1/2}$ where $\Phi(x)$ is the toroidal flux within a given flux surface, and Φ_{max} its maximum value at the last closed flux surface. In Eq. (1-2), the plasma boundary flux has been subtracted from the total poloidal flux so that $\Psi(1,t)=0$. The unknown differential operators $\mathcal{L}_{\alpha,\beta}\{x\}$ and row vectors $L_{\alpha,\beta}(x)$ that characterize the linear response of the system depend on x but are independent of time t, and the input vector $P(t)$ contains the powers from the heating and current drive (H&CD) systems. After projection onto radial basis functions, a lumped-parameter version of the model is obtained, in which all distributed variables and unknown operators reduce to vectors and matrices. The small constant parameter ε (ε <<1) represents the typical ratio between the kinetic and the resistive diffusion time scales. As the order of magnitude of ε is about 0.05 in present-day tokamaks and 0.001 in ITER, we use the theory of singularly perturbed systems both for model identification and controller design [8]. Equations (1-2) thus reduce to a slow dynamic model,

$$\dot{\Psi}(t) = A_S \cdot \Psi(t) + B_S \cdot U_S(t), \qquad X_S(t) = C_S \cdot \Psi(t) + D_S \cdot P_S(t) \tag{3}$$

and a fast dynamic model,

$$\dot{X}_F(t) = A_F \cdot X_F(t) + B_F \cdot P_F(t) \tag{4}$$

where the vector U, containing inputs P and V_{ext}, and all the kinetic variables contained in X are to be split into a slow and a fast component labeled by subscripts S and F, respectively ($X=X_S+X_F$). Details concerning this approximation and the identification of a two-time-scale plasma response model from experimental or simulated data are given in references [4, 5].

3. Model-based Control Designs

A near-optimal controller was obtained by applying the theory of singular perturbations to optimal control [8], a technique that properly decouples the two time scales when the parameter ε is sufficiently small (Eq. 2). The algorithm uses two main feedback loops [4]: *(i)* a proportional-plus-integral (PI) control loop which drives the system on the resistive time scale towards a self-consistent equilibrium state that minimizes a given cost function; *(ii)* a fast proportional control loop that regulates the transient behaviour of the kinetic variables on the plasma confinement time scale when they are subject to rapid disturbances.

The composite control algorithm provides $U(t) = U_S(t) + U_F(t)$, the best $O(\varepsilon^2)$ solution to the minimization of the cost functional (the + superscript is used for transposition):

$$J\left[U(t)\right] = \int_0^\infty dt \left\{ \left[\Delta\Psi^+(t) \quad \Delta X^+(t)\right] \cdot Q \cdot \begin{bmatrix} \Delta\Psi(t) \\ \Delta X(t) \end{bmatrix} + \alpha_\xi^2 \xi^+(t) \cdot \xi(t) + U^+(t) \cdot R \cdot U(t) \right\} \tag{5}$$

where the vectors $\Delta\Psi$ and ΔX contain the error signals, $\xi(t) = \int_0^t K_\xi \cdot \begin{bmatrix} \Delta\Psi(\tau) \\ \Delta X(\tau) \end{bmatrix} d\tau$, and U(t) is the actuator vector. Q and R are positive-definite matrices and K_ξ is an appropriate rectangular scaling matrix that characterizes integral control. When K_ξ and α_ξ^2 are properly chosen, the integral feedback control drives the system towards the self-consistent equilibrium that minimizes the steady state cost function,

$$I_\infty = \int_0^1 \left[\Psi_\infty(x) - \Psi_{\text{target}}(x) \right]^2 dx + \lambda_{kin}^2 \int_0^1 \left[X_\infty(x) - X_{target}(x) \right]^2 dx \tag{6}$$

and is achievable with the given actuators [4]. λ_{kin} is a weighting parameter for kinetic control. The number of positive singular values of K_ξ is the order of the controller. An anti-windup scheme is applied to the output of the controller when actuator saturation occurs.

The second controller used in the experiments is a mixed-sensitivity controller reported in detail in [6] and is obtained by applying the theory of robust control. A singular value decomposition (SVD) of the steady-state plasma response model is carried out to decouple the system and identify the most relevant control channels. The dynamic plasma response model is then explicitly integrated into the synthesis of a feedback controller that minimizes the reference tracking error and rejects external disturbances with minimal control energy and guaranteed bounds of robustness. The feedback controller, which corrects the time-varying feedforward control inputs, is then augmented with an anti-windup compensator, which keeps the given profile controller well-behaved in the presence of magnitude constraints in the actuators and leaves the nominal closed-loop unmodified when no saturation is present.

4. Closed-loop Control of the Poloidal Flux Profile on DIII-D

The chosen reference plasma state around which the data-driven models were identified on DIII-D was that of a 1.8 Tesla, β_N-controlled AT scenario, at a central plasma density, $n_{e0} \approx 5\times10^{19}$ m^{-3} and plasma current, I_p = 0.9 MA. The scenario had been developed to combine non-inductive current fractions near unity with normalized pressure $3.5 < \beta_N < 3.9$, bootstrap current fractions larger than 65%, and a normalized confinement factor, $H_{98(y,2)} \approx 1.5$ [1].

Neutral beam injection (NBI) and electron cyclotron current drive (ECCD) systems provided the H&CD sources for these experiments. The magnetic profiles were obtained in real time from a complete equilibrium reconstruction using motional Stark effect (MSE) data from two dedicated beamlines to provide information on the current density profile. These beamlines injected in the co-current direction a baseline power of 2 MW and were not used for control. Other available beamlines and gyrotrons were grouped to form six independent H&CD actuators: *(i)* on-axis co-current NBI power, P_{CO}, *(ii)* off-axis co-current NBI power, P_{OA}, *(iii)* counter-current NBI power, P_{CNT}, *(iv)* balanced NBI power, P_{BAL}, *(v)* total ECCD power from up to 6 gyrotrons in a fixed off-axis current drive configuration, P_{EC}, and *(vi)* either V_{ext} or the plasma current, I_p. A combined feedforward and feedback control of the central ohmic coil voltage and current was effective in providing the requested surface loop voltage.

In the first experiment using near-optimal control, the poloidal flux profile, $\Psi(x)$, was controlled from t=2.5 s to t=6 s (i. e. starting after a 1 s current flat-top), with four available actuators : P_{CO}, P_{BAL}, P_{EC} (with only 5 gyrotrons) and V_{ext}. The Ψ vector consisted of the values of $\Psi(x)$ at 9 radii (x=0.1, …0.9) and the Q-matrix was chosen in such a way that the quadratic $\Psi^+ Q \Psi$ was approximately equal to the integral of $\Psi(x)^2$ from x=0.1 to 1. K_ξ was a pseudo-inverse of the steady state gain matrix of the model, limited to its 2 principal components so that the controller order was 2. Three different values of the integral weight parameter, α_ξ, were used (4, 10 and 25). The profile control phase started at t=2.5 s, i.e. 1 s after the end of the initial current ramp-up, and the best controller performance was obtained with α_ξ = 25. This is illustrated on FIG. 1, which shows the time traces of $\Psi(x)$ at x=0.1, …0.9 in different colors (the piecewise-linear target traces are also represented with the same colors) and the $\Psi(x)$ profile at

t=2.5 s, 4 s and 6 s, respectively, for shot #146416. The time evolution of the actuators is also displayed.

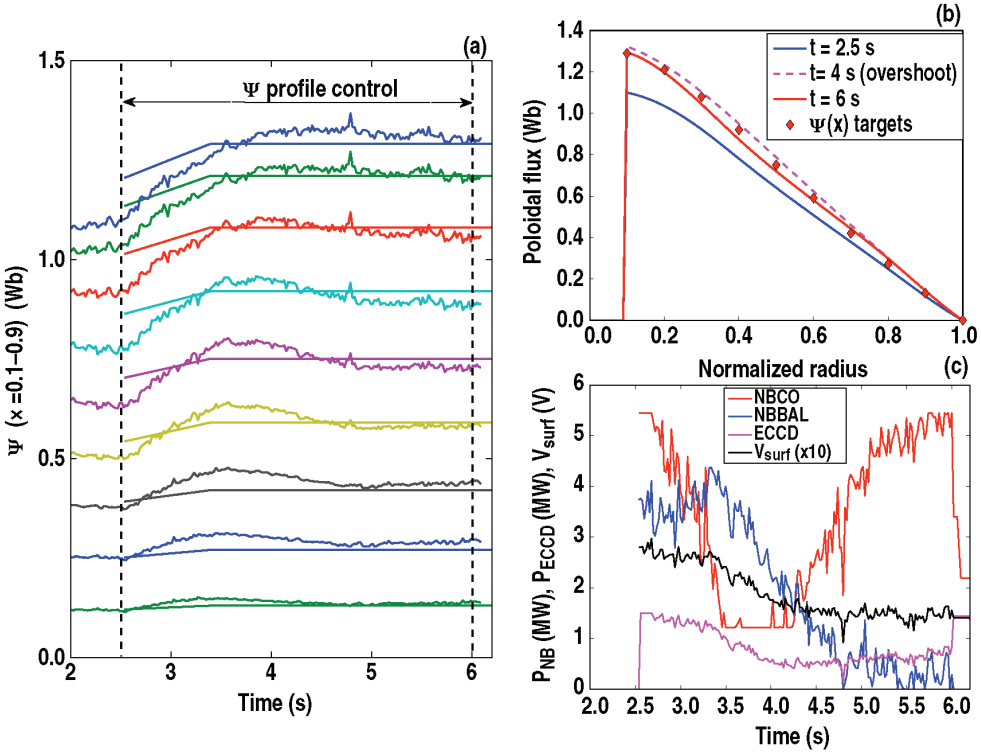

FIG. 1. Shot #146416. (a) Ψ(x) at x=0.1,...0.9 vs time and target traces (piecewise-linear). (b) Ψ(x) profile at at t=2.5 s, 4 s and 6 s and target profile (stars). (c) Actuators vs time.

5. Simultaneous Control of the Current Profile and β_N on DIII-D

5.1. Control of the poloidal flux profile and β_N

Simultaneous control of the poloidal flux profile and of the normalized pressure parameter, β_N, was performed using the near-optimal two-time-scale algorithm described in Sec. 3 and 4. The counter-current NBI actuator, P_{CNT}, was available in this experiment, so a total of 5 independent actuators were used, with also a little more power in the ECCD actuator from 6 gyrotrons. The Ψ vector still consisted of the values of Ψ(x) at 9 radii (x=0.1, …0.9) and the Q matrix was chosen as before with an additional diagonal element equal to λ_{kin}^2 corresponding to the weight on β_N control. Based on the magnitude of the steady state gain matrix of the model, this weight was chosen as λ_{kin} = 0.3. With this choice for λ_{kin}, controllers of order 2 and 3 were tested, starting from t= 2.5 s. The order-3 controller with α_ζ =10 showed the best performance. Then, the start time of the control phase was moved earlier from 2.5 s to 1 s, i.e. during the initial current ramp-up phase. The controller performed well, although the data-driven model was identified using only data after 2.5 s, i.e. after the plasma equilibrium had relaxed from the initial current ramp-up phase [5]. Figure 2(a) and 2(b) show the time traces of Ψ(x) at x=0.1, …0.9 tracking the nine piecewise-linear target traces, and the Ψ(x) profile at t=0.5 s, 2.4 s and 5 s, respectively, for shot #146463. Figure 2(c) shows β_N tracking its 2.5 target, the plasma current floating slightly above 1 MA, and the MHD activity versus time. Despite an m/n=2/1 MHD mode from t=2.3 s to the end, and the saturation of the balanced injection actuator between t=2 s and t=4 s, simultaneous ψ(x) and β_N control was successful.

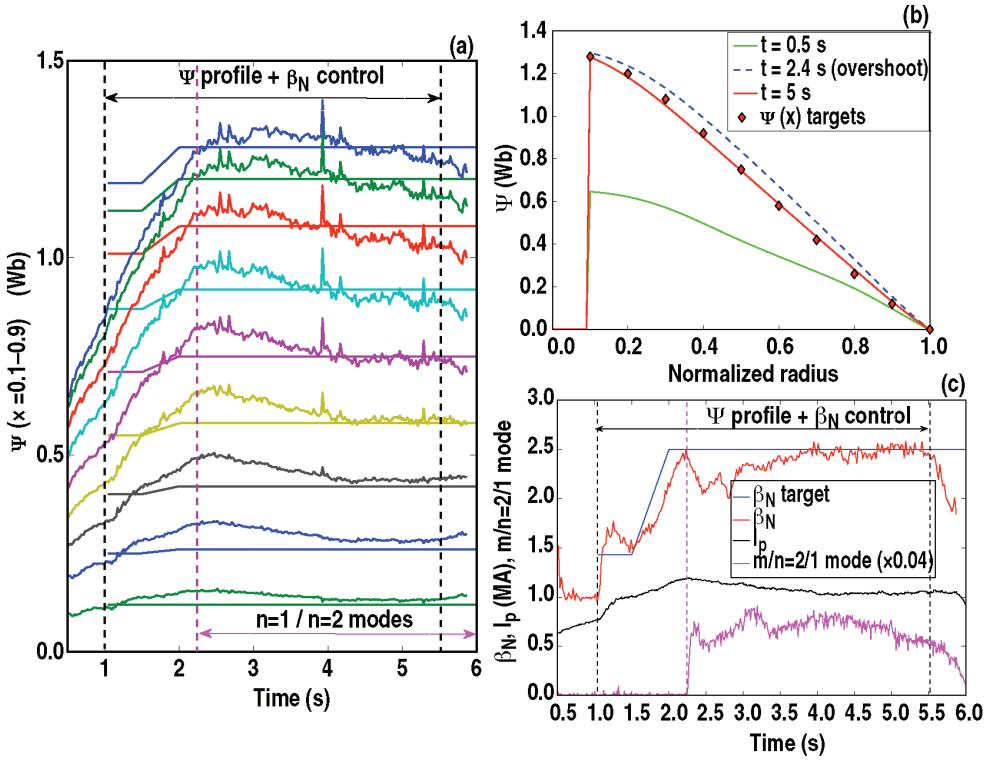

FIG. 2. . Shot #146463. (a) Ψ(x) at x=0.1,…0.9 vs time and target traces (piecewise-linear). (b) Ψ(x) profile at t=0.5 s, 2.4 s and 5 s and target profile (diamonds). (c) β_N (red), β_N target (blue), plasma current (black) and m/n=2/1 MHD mode amplitude (magenta).

5.2. Control of the safety factor profile and β_N

The safety factor profile, defined as $q(x) = -d\Phi(x)/d\Psi(x)$, was also controlled, through its inverse, $\iota(x)$. Control of $\iota(x)$ and simultaneous control of $\iota(x)$ and β_N were first performed through a mixed-sensitivity robust control algorithm (Sec. 3). Here the actuators were P_{CO}, P_{CNT}, P_{BAL}, P_{EC} and I_p. Figure 3 shows an example where the controller was switched on from t=2.5 s until t=4.75 s and from t=5 s until t=6 s. Disturbances in the actuators were artificially introduced at t=3 s. The target and achieved values of $\iota(x)$ at x = 0.2, 0.4, 0.5, 0.6, 0.8 and of β_N can be compared. Good control was observed, with a clear recovery after the injection of disturbances and the momentary shutdown of the feedback controller.

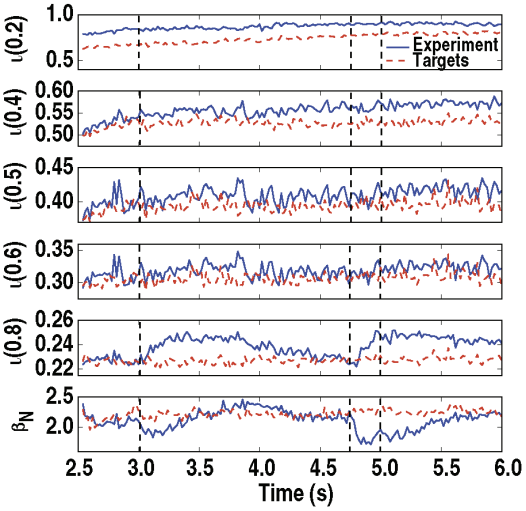

Fig. 3. Shot #147707: Experimental (blue) and target (red) traces of ι(x) at x=0.2, 0.4, 0.5, 0.6, 0.8 and β_N. Disturbances are introduced at t=3 s and the controller is off between 4.75 s and 5 s.

In another experiment, the near-optimal controller was used and the actuators included off-axis NBI power, P_{OA}, together with P_{CO}, P_{CNT}, P_{EC} and V_{ext}. The $\iota(x)$ target corresponded to a broad flat q-profile between x = 0 and $x \approx 0.6$, with a minimum value, q_{min}=1.7. The magnetic field, 1.7 T, was lower than it was when the model had been identified (1.8 T) and its direction was reversed. The control phase for $\iota(x)$ began at 1 s, during ramp-up, the radial control window was $0.05 \le x \le 0.6$ and β_N was not controlled. The controller satisfactorily

tracked the $\iota(x)$ target profile for $x \leq 0.6$ (Fig. 4), until the plasma current reached about 1.2 MA. The q-profile is shown on Fig. 4(b) at t = 1 s, 2 s and 3 s together with the target values at t=2 s and 3 s. At t ≈ 2.7 s the controller surface loop voltage request became negative but, for technical reasons due to a wrong setting of the premagnetization in this discharge, the request could not be followed [Fig. 4(c)] and control was lost. Nevertheless, without any feedforward command except the constant reference surface voltage and powers around which the model was linearized, the controller successfully ramped the plasma current up while tracking the given $\iota(x)$ or q(x) target profile.

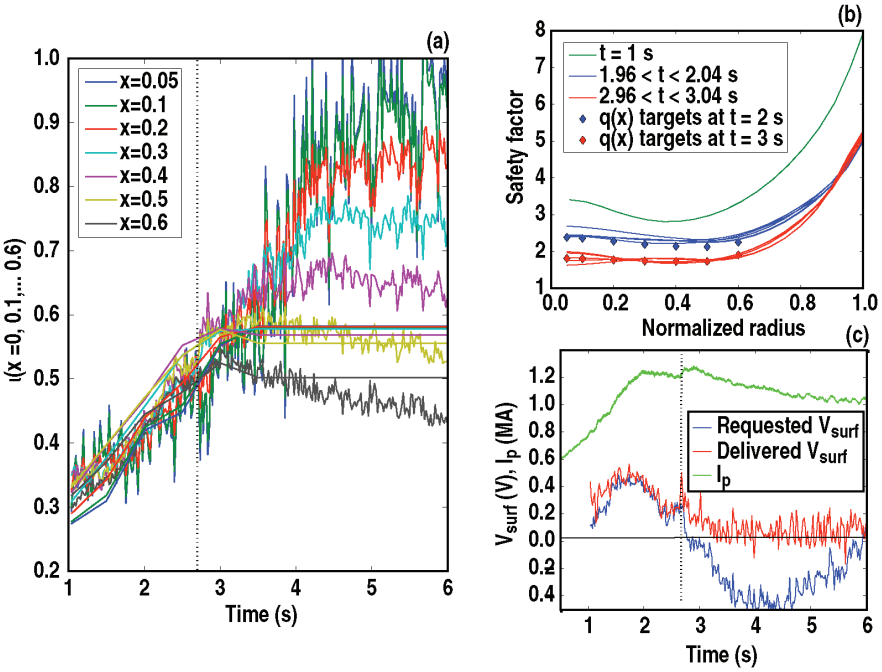

Fig. 4. Shot #150083. (a) ι(x) at x=0.05, 0.1, 0.2, ...0.6 vs time and target traces (piecewise-linear). A vertical line shows loss of control at 2.7 s. (b) q-profiles at t=1 s, 2 s and 3 s and target values at t=2 s and 3 s. (c): Plasma current (green), requested (blue) and delivered (red) V_{surf} vs time.

6. Current Profile and Burn Control Simulations in ITER

In ITER hybrid and steady state scenarios, profile control and burn control cannot be dissociated because the improved confinement and stability that is required in these scenarios is a natural outcome of the profile shaping. To complement the experiments reported above, the near-optimal control algorithm (Sec. 3) has been coupled to a simplified transport code, METIS [10], to simulate integrated current profile control and burn control in ITER. METIS computes the time evolution of the global plasma quantities for given waveforms of the input parameters. It solves the current diffusion equation taking into account an approximate equilibrium evolution, and uses a simplified treatment of the distributed sources while retaining the main plasma nonlinearities. In the example shown below, we consider a hybrid scenario that was first obtained from open loop METIS simulations [11] with a plasma current I_p=12 MA, a magnetic field B=5.3 T, and a fusion power of 550 MW. The control actuators were NBI (2 actuators with 16.5 MW each), ECRH, ICRH and LHCD with 20 MW each, and the surface loop voltage. Closed-loop simulations using the near-optimal two-time-scale algorithm showed effective control of the $\Psi(x)$ profile and P_α for different preset target values (Fig. 5) [9]. This constitutes an excellent basis for the development of integrated control in ITER using more accurate plasma simulators.

7. Conclusion

A generic method for integrated profile control based on semi-empirical data-driven models is being experimentally tested on DIII-D and simulated on ITER. These models can be identified either from experimental or simulation data and provide, for control purposes, a readily available alternative to first-principle plasma modeling. Control of the poloidal flux or safety factor profile and, simultaneously, of β_N was demonstrated on DIII-D using either a robust control algorithm or a near-optimal two-time-scale algorithm. Simulations of an ITER hybrid scenario showed that burn control can also be integrated in the control scheme. More extensive experimental and numerical investigations along these principles could therefore lead to the rapid development of integrated plasma control for advanced scenarios in ITER.

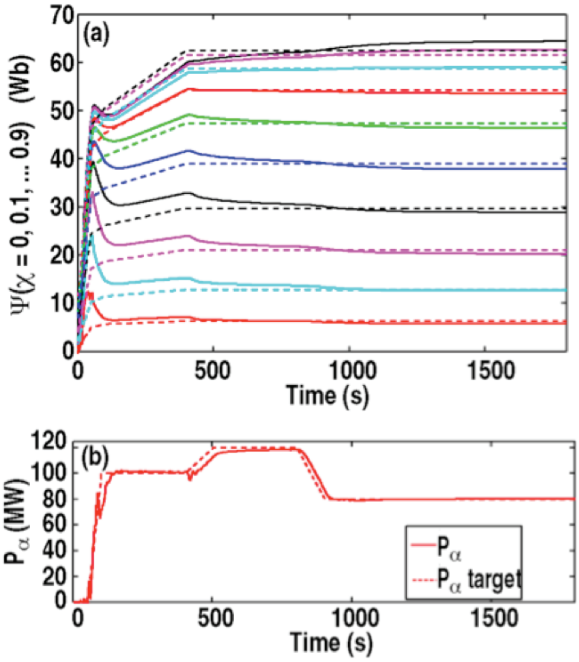

Fig. 5. Burn control in ITER (METIS simulation, hybrid scenario). (a) Ψ(x) at x=0, 0.1, ... 0.9 vs time (solid) and target traces (dashed). (b) Alpha-particle power vs time (solid) and target trace (dashed).

Acknowledgments

This work was supported by the European Communities under contract of Association between EURATOM and CEA, was carried out within the framework of the European Fusion Development Agreement, and of the US Department of Energy under DE-FC02-04ER54698, DE-FG02-09ER55064, DE-FG02-92ER54141, DE-AC52-07NA27344, DE-AC05-00OR22725, and DE-FG02-04ER54761. The views and opinions expressed herein do not necessarily reflect those of the European Commission. The first author is very grateful to the DIII-D Team for their support and hospitality.

References

[1] HOLCOMB, C.T., et al., Phys. of Plasmas **16** (2009) 056116.
[2] OYAMA, N., and the JT-60 Team, Nucl. Fusion **49** (2009) 104007.
[3] LITAUDON, X., et al., Nucl. Fusion **51** (2011) 073020.
[4] MOREAU, D., et al., Nucl. Fusion **48** (2008) 106001.
[5] MOREAU, D., et al., Nucl. Fusion **51** (2011) 063009.
[6] SHI, W., et al., Proc. 2012 American Control Conference, Montreal (2012), FrA16.3.
[7] BARTON, J.E., et al., This conference, paper EX/P2–09.
[8] KOKOTOVITCH, P.V., et al., "Singular Perturbation Methods in Control: Analysis and Design," Academic Press, London (1986).
[9] LIU, F., *et al.*, Proc. 39th EPS Conference on Plasma Physics, Stockholm (2012) P1.063.
[10] ARTAUD, J.F., *et al.*, Nucl. Fusion **50** (2010) 043001.
[11] GARCIA, J., Private Communication March (2012).